Science of the Total Environment 587–588 (2017) 273–281

2561

Contents lists available at ScienceDirect

Science of the Total Environment

journal homepage: www.elsevier.com/locate/scitotenv

Simplifying field-scale assessment of spatiotemporal changes of soil salinity

Elia Scudiero [a,b,*], Todd H. Skaggs [b], Dennis L. Corwin [b]

[a] University of California Riverside, Department of Environmental Sciences, Riverside, CA, USA
[b] USDA-ARS, United States Salinity Laboratory, Riverside, CA, USA

HIGHLIGHTS

- Calibrated apparent electrical conductivity (EC_a) can be used to estimate soil salinity.
- A t-ANOCOVA calibration was used to monitor salinity using limited soil sampling.
- The t-ANOCOVA calibration was compared to established EC_a calibration approaches.
- The t-ANOCOVA calibration was reliable, especially at low salinity values.

GRAPHICAL ABSTRACT

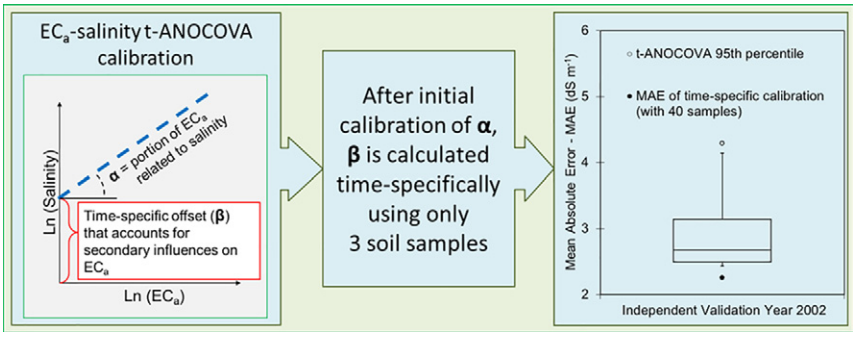

ARTICLE INFO

Article history:
Received 6 December 2016
Received in revised form 15 February 2017
Accepted 16 February 2017
Available online 27 February 2017

Keywords:
Soil spatial variability
Soil salinity
Electromagnetic induction
Mapping
Monitoring

ABSTRACT

Monitoring soil salinity (EC_e) is important for planning and implementing agronomic and irrigation practices. Salinity can be measured through soil sampling directed by geospatial measurements of apparent soil electrical conductivity (EC_a). Using data from a long-term (1999–2012) monitoring study at a 32.4-ha saline field located in California, USA, two established field-scale approaches to map and monitor soil salinity using EC_a are reviewed: one that relies on a single EC_a survey to identify locations that can be repeatedly sampled to infer the frequency distribution of EC_e; and another based on repeated EC_a surveys that are calibrated, each time, to EC_e estimation using ground-truth data from soil samples. The reviewed approaches are very accurate and reliable, but require extensive soil sampling. Subsequently, we propose a novel approach – temporal analysis of covariance (t-ANOCOVA) modeling – that results in accurate spatiotemporal salinity estimations using EC_a surveys with a significant reduction in the number of soil samples needed for calibration of EC_a to EC_e. In this modeling framework, the EC_e-EC_a relationship is described with a log-transformed linear function. The regression slope indicates the magnitude of the contribution of EC_e to EC_a and is assumed to remain constant over time, while the intercept represents the secondary factors influencing EC_a that are not related to EC_e (e.g., soil tillage). Once the t-ANOCOVA slope is established for a field, in subsequent surveys as few as three soil samples are used to estimate a time-specific t-ANOCOVA intercept so that EC_a measurements can be converted to EC_e estimations. Our results suggest that this approach is reliable at

Abbreviations: t-ANOCOVA, temporal analysis of covariance; EC_a, apparent soil electrical conductivity (dS m^{-1}); EC_e, electrical conductivity of the saturation extract (dS m^{-1}); EM_h, electromagnetic induction measurement in the horizontal coil configuration; EMI, electromagnetic induction; EM_v, electromagnetic induction measurement in the vertical coil configuration; MAE, mean absolute error; OLS, ordinary least squares; RSSD, response surface sampling design; SSMU, site-specific management units; TSC, time-specific calibration; WSJV, west side of the San Joaquin Valley.

* Corresponding author at: University of California Riverside, Department of Environmental Sciences, Riverside, CA, USA.
E-mail addresses: elia.scudiero@ars.usda.gov, scudiero@dmsa.unipd.it (E. Scudiero).

http://dx.doi.org/10.1016/j.scitotenv.2017.02.136
0048-9697/Published by Elsevier B.V.

low salinity values (i.e., where common crops can grow). The t-ANOCOVA approach requires further validation before real-world implementations, but represents a significant step towards the use of EC_a mobile sensor technology for inexpensive soil salinity monitoring at high temporal resolution.

Published by Elsevier B.V.

1. Introduction

Managing agricultural soil salinity is crucial to sustaining future food production. Soil salinity strongly limits global crop yields (FAO and ITPS, 2015). Over 20% of global irrigated farmland is affected by soil salinity (Tanji and Wallender, 2012; Wicke et al., 2011). More than half of that 20% belongs to four countries: China, India, Pakistan, and the United States of America (FAO and ITPS, 2015). Salinity is typically managed by irrigating soils beyond the consumptive water use of plants, leaching from the root zone soluble salts that would otherwise harm plant growth (e.g., sodium, chloride) due to osmotic effects, specific ion toxicity effects, nutrient imbalances, and influences on tilth and permeability. Reliable information on salinity levels of the soil root-zone (e.g., 0 to 0.9–1.5 m depth) is essential for developing salinity management strategies, particularly when water resources are limited.

The complex spatial patterns of salinity usually found on agricultural lands (Lesch et al., 1992) make it difficult to map salinity using grid or random sampling since tremendous numbers of samples (e.g., hundreds per field) are necessary. Clearly, there is a cost issue related to monitoring the spatiotemporal changes of soil salinity at field scale (e.g., <1 km^2) over multiple fields. By using soil apparent electrical conductivity (EC_a, dS m^{-1}) measurements from mobile on-the-go sensors, expenses can be notably lowered (Lesch, 2005). Soil EC_a is influenced by several properties, including: water content, texture, and soil salinity (Corwin and Lesch, 2005; Doolittle and Brevik, 2014). To estimate salinity, EC_a measurements must be site-specifically calibrated to ground-truth measured soil salinity, generally measured as electrical conductivity of the saturation extract (EC_e), by establishing a linear model between EC_e and EC_a (Lesch, 2012). Because it can be easily mobilized and coupled with GPS systems, EC_a is measured intensively with tens of thousands of sampling locations per field.

Geospatial EC_a measurements serve as a surrogate to characterize the spatial variability of soil properties correlated to EC_a at a given site (Corwin and Lesch, 2003; Corwin and Lesch, 2005). In instances where salinity dominates the EC_a measurement (i.e., $EC_a > 2$ dS m^{-1}), the spatial variability of EC_a will represent the spatial variability of soil salinity (Corwin and Lesch, 2013). Therefore, the EC_a surveys can be used to select representative (in terms of inferential statistics) soil sampling locations that will reflect the range and spatial variation in georeferenced EC_a measurements (Corwin and Lesch, 2005). Model-based sampling design algorithms, such as the response surface sampling design (RSSD) (Lesch et al., 2000; Lesch, 2005), can be used to identify the optimal representative soil sampling locations. The RSSD identifies soil sampling locations so that the frequency statistics of the ancillary information used, be it EC_a (Lesch, 2005) or remote sensing imagery (Fitzgerald et al., 2006) or radar data (Guo et al., 2015), is fully represented. Concurrently, the RSSD maximizes the distance between selected soil sampling locations. This latter step is directed to avoid (short-scale) autocorrelation of ordinary least squares (OLS) regression residuals (Hengl et al., 2003; Lesch and Corwin, 2008).

The first objective of this manuscript is to discuss two established approaches in which geospatial measurements of EC_a are used to monitor soil salinity at field scale. The first methodology consists of using an initial EC_a survey to identify representative soil sampling locations that are sampled for EC_e over time at selected time intervals. The other consists of surveying the field for EC_a at each sampling time and then calibrating the sensor readings using soil samples taken at the time of the EC_a survey. If the spatial EC_a patterns are unchanged, then the sample locations are the same as those determined in the first EC_a survey. If the spatial EC_a patterns have changed, then new sample locations are identified that reflect the range and spatial variability of the new EC_a survey.

The second objective is to propose a novel salinity monitoring approach based on the assumption of temporal covariance (t-ANOCOVA) of the EC_e-EC_a relationship, which should allow reducing the number of soil samples needed at each monitoring time. The t-ANOCOVA is a temporal application of the ANOCOVA EC_e-EC_a calibration model presented by Corwin and Lesch (2014) and later validated by Corwin and Lesch (2016) and Scudiero et al. (2016). After an initial calibration that requires from a half to several dozen soil samples per field depending on the extent of the variability, the t-ANOCOVA approach only requires as few as three soil samples to calibrate the EC_a measurements taken at subsequent monitoring times.

2. Theoretical background

2.1. Temporal covariance of the EC_e-EC_a relationship

Apparent soil electrical conductivity measurements can be expressed as a multiplicative function of salinity, water content, and soil tortuosity, which depends on several soil properties, including soil texture, particle pore distribution, density and particle geometry, and organic matter content. According to Archie's Law (Archie, 1942), and other similar models (e.g., Rhoades et al. [1976]), EC_a may be expressed as a function of pore-water salinity (EC_p), soil water content, and other soil-specific parameters:

$$EC_a = \frac{EC_p \times \phi^m \times S^n}{k} \quad (1)$$

where ϕ is soil porosity, S is the relative saturation, and k, m, and n are fitting parameters that are dependent on soil texture, organic carbon content, and other physical and chemical properties (Allred et al., 2008). However, Eq. (1) is not applicable when soil is too dry because the water pathways for electrical conductivity are not continuous. As a rule of thumb, Corwin and Lesch (2013) suggest that volumetric water content should be at least 70% of field capacity when the EC_a survey is carried out.

Because the pore-water electrical conductivity, EC_p, can generally be expressed as a linear function of the total ion content in the soil (Rhoades et al., 1989), salinity (EC_e) can be expressed as a function of EC_a with a multiplicative error model (Corwin and Lesch, 2014):

$$EC_e = \beta \times EC_a^{\alpha} \times \varepsilon^* \quad (2)$$

where α and β are coefficients that subsume ϕ, S, k, m, and n; and ε^* is a multiplicative error component. In Eq. (2), the error component is a function of the ratio between EC_e and the explanatory term of the equation (Baskerville, 1972; Tian et al., 2013).

After a log transformation of Eq. (1), the EC_a-EC_e relationship is:

$$\ln(EC_e) = \ln(\beta) + \alpha \times \ln(EC_a) + \varepsilon \quad (3)$$

where ε is a random additive error component, equal to $\ln(\varepsilon^*)$. Eq. (3) can be parameterized using an OLS approach, provided the underlying assumptions (including residuals being normally distributed and spatially independent) are respected (Lesch and Corwin, 2008).

The influence of salinity on EC_a readings is reflected in the slope (α) of Eq. (3). The effects not due to salinity but to other soil properties (e.g.,

water content, bulk density) are represented by the regression intercept. This approach, referred to as an analysis of covariance (ANOCOVA) approach, has been previously used to map salinity at multiple fields using regional values of α (Corwin and Lesch, 2016; Corwin and Lesch, 2014; Scudiero et al., 2016). In these studies, a group of calibration fields were selected having broad ranges of salinity and differing soil types. Intense EC_a surveys were carried out. At each field, soil was sampled according to the spatial variability of EC_a. A common (i.e., regional) α coefficient was established. The determination of $\ln(\beta)$ was field-specific. Using the regional α coefficient, EC_e can be estimated at new sites by estimating a local (i.e., site-specific) $\ln(\beta)$; consequently, soil sampling labor is minimized. Ideally, only one data point is needed for estimating the local intercept. However, error in the intercept estimation may be sizeable when using a single data point. By sampling soil at three random locations and then averaging the three derived intercepts, the site-specific $\ln(\beta)$ should be more representative of the entire field.

An alternative approach is to use Eq. (3) in a spatiotemporal framework. We refer to this approach as temporal analysis of covariance (t-ANOCOVA). We discuss the case when the coefficient α is calculated at an initial salinity survey and then used to calibrate the EC_e-EC_a relationship at other times. For each consecutive survey, an intense EC_a survey is carried out and soil is sampled at three locations for the calculation of a time-specific $\ln(\beta)$.

3. Materials and methods

The salinity assessment methodologies are discussed using data from a long-term study on salinity changes under different irrigation regimes. The study was carried out over a 32.4 ha saline field (latitude 36°11′24.827″N, longitude 119°52′45.455″W) in Kings County, California, with a portion of the data published by Corwin et al. (2008) and Corwin (2012). Fine, montmorillonitic, thermic, Typic Natrargid (Arroues and Anderson, 1986) clay loam soils are found at the site. Additional details on the study site can be found in (Corwin et al., 2003). Field surveys were conducted at the site in 1999 (EC_a and EC_e), 2002 (EC_a and EC_e), 2004 (EC_a and EC_e), 2009 (EC_e only), 2011 (EC_a and EC_e), and 2012 (EC_a and EC_e). The 2012 field survey was not discussed by Corwin (2012). The 2012 EC_a and EC_e surveys together with those from 21 other fields scattered throughout the western San Joaquin Valley (WSJV) were used by Scudiero et al. (2016) to estimate the ANOCOVA α coefficient for the WSJV.

3.1. Apparent electrical conductivity surveys and soil sampling

EC_a surveys were conducted using mobile electromagnetic induction (EMI) equipment in August 1999, April 2002, November 2004, April/May 2011, and September 2012. The 1999 survey consisted of 384 EC_a measurements acquired over a grid-like sampling scheme, with measurements taken approximately 20–30 m apart. A figure of this EC_a survey is featured in the paper by Corwin et al. (2003). EC_a measurements were taken with an EM38 Electrical Conductivity Meter (Geonics Ltd., Mississauga, Ontario, Canada). Measurements were taken in the horizontal (EM_h) and vertical (EM_v) dipole modes to provide shallow (0–0.75 m) and deep (0–1.5 m) measurements of EC_a, respectively. The sampling locations were georeferenced with sub-meter accuracy using a Trimble Pro-XRS GPS system (Trimble, Sunnyvale, CA, USA).

Subsequent EC_a surveys were more intensive. In 2002, 2004, 2011, and 2012, EC_a was measured with a dual-dipole EM38 (acquiring simultaneous EM_h and EM_v readings) coupled with a sub-meter accuracy GPS and mounted on a mobile, non-metallic, platform. EC_a was measured every ~4 m along parallel transects spaced roughly 8 m apart, totaling over 20,000 locations for each survey. The volumetric water content was close to field capacity when all EC_a surveys were conducted. Fig. 1 shows the EC_a survey for 2002. The EC_a spatial patterns were similar to those in 2004, 2011, and 2012.

Using the EC_a data from the 1999 EMI survey and ESAP software (Lesch et al., 2000), 40 soil sampling locations were selected to represent the frequency distribution of the bivariate EMI survey data, and to be allocated across the field to avoid spatial clustering.

Soil cores were taken at the 40 sites, in the days following the EC_a surveys and in August 2009. At each site (Fig. 1), soil-cores were taken at 0.3 m increments to a depth of 1.2 m. Additionally, in 2002, 60 locations were sampled in two subsections of the field (Fig. 1). These locations, which will be used as independent validation data, were selected using the RSSD. All soil cores were kept in refrigerated storage prior to air-drying and sieving (2-mm sieve), which occurred within a few days after their collection. Soil samples were then analyzed for soil salinity (EC_e) and other (see Corwin [2012]) physical and chemical properties.

3.2. Soil salinity monitoring

3.2.1. Characterizing EC_e using EC_a-directed soil sampling

If the frequency distribution of EC_e can be described by that of EC_a, then a representative subsample of EC_a can be used to describe the EC_e population. This is referred to as EC_a-directed soil sampling (Corwin and Lesch, 2005; Lesch, 2005).

In the case where the relative spatial structure of EC_a is stable across a site over time, then the same soil sampling locations can be revisited over time because the EC_a frequency distribution remains unchanged. The 1999 soil sampling scheme was sampled over time to estimate the frequency distribution of EC_e at the site. The validity of this approach was verified by comparing the EC_a frequency distribution of the entire field over the 40 soil sampling locations with a (two-sample) Kolmogorov–Smirnov test.

3.2.2. EC_e-EC_a linear regression and spatial interpolation.

Site-specific linear relationships between EC_a and EC_e can be established, so that EC_e can be estimated at all locations where only EC_a is measured. Multiple OLS regression can be used to calibrate the EC_e-EC_a relationship. Ordinary Least Squares regression analysis makes several key assumptions, including: no or little multicollinearity between explanatory variables, homoscedasticity, and normality and spatial randomness of the residuals (Achen, 1982). When dealing with spatial datasets, particular attention should be given to avoiding spatial autocorrelation of the residuals (Cordioli et al., 2017; Lesch and Corwin, 2008). To do so, model-based sampling scheme optimization methods, such as the RSSD, should be used. This assumption can be tested using the Moran's *I* Test for Residual Spatial Autocorrelation (Cliff and Ord, 1981).

Often, spatial autocorrelation in the residuals can be avoided by including information on trend surface parameters (i.e., x and y coordinates) in the OLS regression (Lesch, 2012). Salinity is estimated as:

$$\ln(EC_e) = \gamma_0 + \gamma_1 \times \ln(EM_v) + \gamma_2 \times \ln(EM_h) + \gamma_3 \times x + \gamma_4 \times y + \varepsilon \quad (4)$$

where γ_0, γ_1, γ_2, γ_3, and γ_4 represent the empirical regression model coefficients; x and y are the easting and northing UTM coordinates (m), and ε is random the error term. If there was no multicollinearity between EM_v and EM_h, then Eq. (4) was unchanged. Otherwise, multicollinearity was addressed by removing the least significant of either EC_a measurements or by using the principal components (PCA1 and PCA2) of EM_v and EM_h. Principal component analysis was carried out with Statistica 12 (StatSoft Inc. Tulsa, Oklahoma, USA). For further detail on the use of OLS regression for prediction of spatial soil property information from ancillary sensor data, refer to Lesch and Corwin (2008) and (Lesch, 2012). A walkthrough application of this mapping approach is provided by Corwin and Scudiero (2016).

The EC_e-EC_a calibration regressions were established for each sampled depth. Once EC_e was estimated at all EC_a survey locations simple kriging, based on spherical experimental semivariograms, was used to

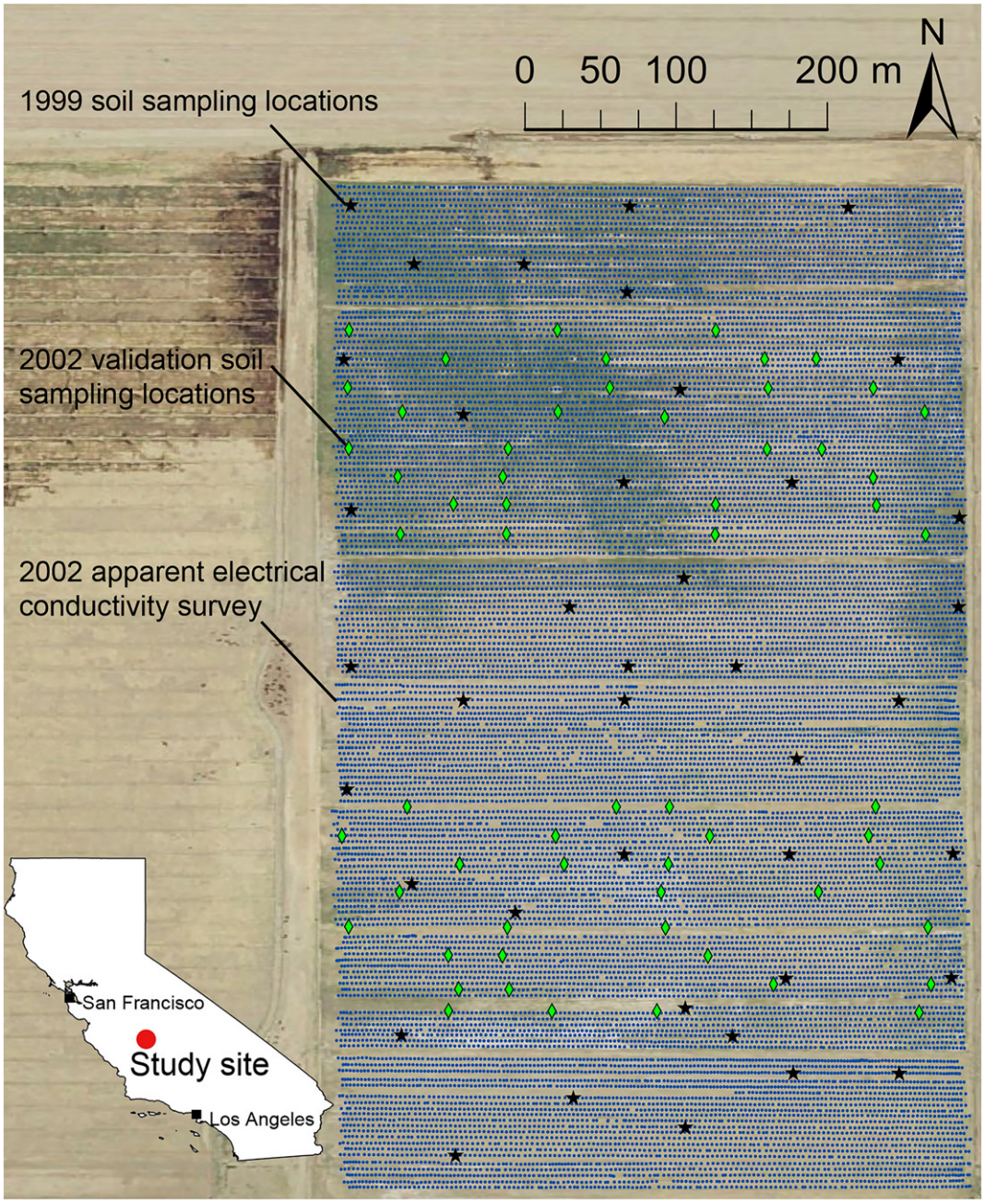

Fig. 1. Map of the study site, located in central California (USA). The apparent electrical conductivity (EC_a) survey of 2002, the EC_a-directed soil sampling scheme of 1999 (and repeated in following surveys), and the 60 validation locations sampled in 2002 are depicted with dots, stars, and diamonds respectively.

map salinity across the field using ArcMap 10.1 (ESRI, Redlands, CA, USA). Each kriging surface had a spatial resolution of 2 × 2 m. The EC_e maps were stacked according to their depth interval. Three-dimensional spatiotemporal changes were depicted using selected 200-m long cross sections having vertical × horizontal resolution of 0.3 × 2 m. The cross sections were visualized on Google Earth™ according to Van Noten (2016). This approach is discussed using the changes of soil salinity between the 2002 and 2011 surveys.

3.2.3. EC_e-EC_a t-ANOCOVA

Two t-ANOCOVA approaches were tested, using different α (i.e., the t-ANOCOVA slope) parameters: one local (site-specific) and one from a multiple-field dataset. For this comparison the local slope was calculated from the 2012 survey. The multi-field t-ANOCOVA slope coefficient was taken from the Scudiero et al. (2016) study (α = 0.99 with a standard error of 0.05). Note that the study field was included in the Scudiero et al. (2016) dataset. The EC_a surveys from previous times (i.e., 1999, 2002, 2004, and 2011 surveys) were then used to map salinity with the t-ANOCOVA approach. The t-ANOCOVA intercept was calculated by selecting three random EC_e sampling locations. The t-ANOCOVA model was developed to estimate the average 0–1.2 m soil salinity profile.

Because only three random samples are needed to estimate the t-ANOCOVA intercept, the remaining 37 locations could be employed to validate the t-ANOCOVA EC_e estimations. Validation was done by cross-validation as follows: 1) three locations were selected (no replacement allowed); 2) the t-ANOCOVA intercept was calculated at each of the three points and then averaged; 3) the averaged intercept was used to estimate salinity over the remaining (thirty-seven) sampling locations to independently validate the t-ANOCOVA estimations.

The cross-validation procedure was repeated 9880 times in order to consider all possible unique combinations where three random samples were chosen for the t-ANOCOVA intercept calculation. The frequency distributions of the mean absolute error (MAE, in dS m^{-1}) and of the observed-predicted relationship were retained for further analysis. This procedure was carried out to test the t-ANOCOVA predictions using the 1999, 2002, 2004, and 2011 surveys.

4. Results and discussion

4.1. Characterizing EC_e changes with EC_a-directed soil sampling

At all dates the EC_a measurements were characterized by significant ($p < 0.001$) Pearson r correlation coefficients with soil salinity (Table 1), affirming that EC_a is a proxy to infer the frequency distribution of EC_e at the site.

The Kolmogorov-Smirnov test showed that the frequency distributions of EM_h and EM_v at the 40 soil sampling locations never significantly differed from the field-wide EM_h and EM_v EC_a surveys. This supported the use of the 1999 soil sampling locations as representative of the spatial variability of EC_a throughout the entire experiment. Other authors (Corwin, 2012; Farahani and Buchleiter, 2004; Pedrera-Parrilla et al., 2016) reported that relative spatial patterns of EC_a in uniformly managed farmland remain stable over time because of the influence of texture on water content and solute transport, which subsequently affect the spatial variability of salinity.

Fig. 2 shows the changes at each depth increment, and over the average 0–1.2 m profile, from 1999 to 2012. The changes in salinity are due to different irrigation practices at the site. From 1999 to 2010, the field was irrigated with drainage water and cropped with Bermuda grass (*Cynodon dactylon* (L.) Pers.) for cattle grazing. This irrigation practice resulted in the decrease of salinity in the root-zone (0–1.2 m) and in the general improvement of several soil physical and chemical properties (Corwin, 2012). Due to the historic multi-year drought that hit California in 2010 (Williams et al., 2015), drainage water ceased to be available. Field management was switched to rain-fed in 2010 through 2012. Because of the shallow water table at the site, salinity rapidly increased due to the upward movement of water from the water table to the soil surface returning the field to its original saline-sodic state. During the drought, salt crusts (re-) appeared at the south-west side of the field. In many areas of the field Bermuda grass was naturally outcompeted by invasive halophytic weeds.

4.2. Mapping 3D salinity change with OLS regression

When (spatial) information on soil salinity changes is required across an entire field, geospatial EC_a measurement can be used. Table 2 shows depth- and time-specific relationships between EC_a readings and soil salinity measurements at the forty soil sampling locations. For all regressions (i.e., time-specific calibrations, TSC), the analysis of variance indicated that the F values were highly significant ($p > F$ at < 0.001). Moreover, the explanatory variables of all models were significant at $p < 0.05$ or below. General OLS assumptions were respected. In particular, the Moran's I test for residual autocorrelation did not indicate the presence of any significant spatial structure in the residuals of any of the models in Table 2. The inclusion of a surface trend component was not always needed to avoid spatial autocorrelation in the residuals. These results suggest that, when carrying out TSC regressions, the use of surface trend component should to be assessed for each single case.

The TSC models in Table 2 were used to estimate EC_e, at all four depths and for both years (i.e., 2002 and 2011), at every location where EC_a was measured. Maps of soil salinity were created using the default simple kriging settings in ArcMap 10.1's *Geostatistical Analyst* package. When presenting salinity estimations from regression models and spatial interpolation techniques, information on the prediction errors should be provided to the stakeholders, especially considering the buildup of error in the process (e.g., Nelson et al. [2011]). For the reason of brevity the quality assessment of the cross-section accuracy will not be shown. Ordinary least squares regression followed by kriging of the regressed values is known as *type-B* regression kriging (Odeh et al., 1995). An alternative to this approach is the regression kriging approach described by Hengl et al. (2004), in which the spatial interpolation surface of the regression predictions is added to that of the residuals. Unfortunately, this approach generally requires a large number of soil sampling locations (e.g., hundred per field) so that a semivariogram can be fitted to the residuals. At field-scale the spatial structure of the OLS residuals can be addressed by including a trend surface component

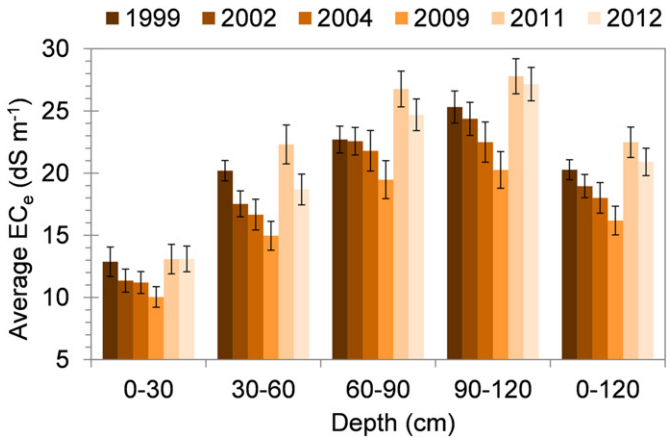

Fig. 2. Histograms showing change in average soil salinity (EC_e) (bars represent standard deviation) for the depth increments 0–0.3, 0.3–0.6, 0.6–0.9, and 0.9–1.2 m and the composite depth 0–1.2 m for the years 1999, 2002, 2004, 2009, 2011, and 2012.

Table 1
Pearson correlation coefficients[a] between apparent electrical conductivity and soil salinity (EC_e) at different depths, in 1999, 2002, 2004, 2011, and 2012.

Year	EMI[b]	0–0.3 m	0.3–0.6 m	0.6–0.9 m	0.9–1.2 m	0–1.2 m
1999	EM_v	0.37*	0.78***	0.71***	0.57***	0.80***
	EM_h	0.52***	0.77***	0.60***	0.42**	0.76***
2002	EM_v	0.63***	0.73***	0.80***	0.69***	0.84***
	EM_h	0.77***	0.85***	0.82***	0.61***	0.89***
2004	EM_v	0.62***	0.82***	0.89***	0.86***	0.89***
	EM_h	0.71***	0.88***	0.89***	0.81***	0.91***
2011	EM_v	0.77***	0.81***	0.80***	0.73***	0.89***
	EM_h	0.81***	0.83***	0.76***	0.65***	0.88***
2012	EM_v	0.68***	0.78***	0.82***	0.71***	0.83***
	EM_h	0.73***	0.80***	0.77***	0.61***	0.81***

[a] Significant correlation at the 0.05 (*), 0.01 (**), and 0.001 (***) probability levels.
[b] EM_h, electromagnetic induction measurement (EMI) in the horizontal coil configuration; EM_v, electromagnetic induction measurement in the vertical coil configuration.

Table 2
Ordinary least square regressions estimating (log-transformed) soil salinity. The back-transformed mean absolute error (MAE) for the observed-estimated salinity relationships are reported.

Year	Depth (m)	Explanatory variables[a]	R^2	Back-transformed	
				R^2	MAE (dS m^{-1})
2002	0–0.3	Intercept, x, y, ln(EM_h)	0.78	0.79	1.88
	0.3–0.6	Intercept, x, ln(EM_h)	0.73	0.77	2.53
	0.6–0.9	Intercept, ln(PCA1)	0.72	0.75	1.51
	0.9–1.2	Intercept, ln(PCA1)	0.53	0.53	4.52
2011	0–0.3	Intercept, ln(PCA1), ln(PCA2)	0.63	0.69	3.17
	0.3–0.6	Intercept, ln(EM_h)	0.71	0.70	4.35
	0.6–0.9	Intercept, ln(PCA1)	0.70	0.66	4.21
	0.9–1.2	Intercept, y, ln(PCA1), ln(PCA2)	0.77	0.76	3.60

[a] EM_h, electromagnetic induction measurement in the horizontal coil configuration; EM_v, electromagnetic induction measurement in the vertical coil configuration; PCA1 and PCA2, first and second components of the principal component analysis for EM_h and EM_v.

in the regression modeling, as seen at this study site and in other published work (Huang et al., 2016; Lesch, 2012).

The salinity maps were stacked, and then cross sections were selected and visualized in Google Earth Pro ™ (Version 7.1.5.1557. Google Inc., Menlo Park, California, USA) according to Van Noten (2016) (Fig. 3). In particular, Fig. 3 shows the change of salinity across selected cross-sections between 2002 and 2011: negative changes indicate salt removal due to leaching and positive changes indicate salt accumulation. This visualization method enables producers and other stakeholders to interactively explore the extent of spatiotemporal changes across areas of interest. Ideally, tens of parallel (and crossing) profiles can be created and displayed interactively. Attention should be given to reporting the vertical exaggeration properly. In Fig. 3, the cross-sections have horizontal × vertical cell size of 2 × 0.3 m.

4.3. t-ANOCOVA EC_e estimations

Goodness-of-fit scores in Table 2, in particular the back-transformed MAE values, are a clear indication that TSC can provide accurate salinity estimations from EC_a readings. Soil sampling and laboratory analyses can be costly, especially if information on salinity is needed at a high temporal resolution. For this purpose, the t-ANOCOVA approach is ideal. Using the t-ANOCOVA approach, only three soil samples are needed per field (or portion of farmland under similar management and conditions). This notably decreases soil sampling and laboratory analyses expenses, making the use of EC_a appealing for routine soil salinity monitoring campaigns.

The t-ANOCOVA was first calculated with a local slope, using the 2012 survey data. The 2012 TSC to estimate the average (0–1.2 m) soil salinity at the site was:

$$\ln(EC_e) = 2.33(\pm 0.080) + 0.622(\pm 0.069) \times \ln(EC_a) + \varepsilon \quad (5)$$

Eq. (5) was highly significant ($p > F$ at < 0.001) with a $R^2 = 0.680$ and had no significant spatial bias in its residuals. The regression coefficients were highly significant ($p < 0.001$) and had small standard errors (reported in parenthesis). When back-transformed, the observed-estimated relationship had R^2 of 0.695 and MAE of 3.08 dS m^{-1}. Local scale variability of the EC_a-EC_e relationship, as well as measurement and random errors, may be among the possible reasons why Eq. (5), as well as the equations in Table 2, could not explain a greater portion of the observed variance of soil salinity.

The slope of Eq. (5) was used to estimate soil salinity in 1999, 2002, 2004, and 2011 using only three random soil sampling locations to calculate time-specific t-ANOCOVA intercepts. The remaining 37 locations were used as validation. Fig. 4a shows the frequency distribution of the t-ANOCOVA validations for the 9880 re-sampling iterations, in 1999, 2002, 2004, and 2011. The MAEs of the back-transformed observed-predicted EC_e relationship are reported. The TSC MAE values in 1999 (2.20 dS m^{-1}), 2002 (2.51 dS m^{-1}), 2004 (2.75 dS m^{-1}), and 2011 (2.80 dS m^{-1}) are reported in Fig. 4a for comparison. In a very limited number of cases in 1999, 2002, and 2011, the t-ANOCOVA outperformed the TSC modeling. The median MAE values (i.e., line across boxes) in 1999 (2.55 dS m^{-1}) and in 2011 (3.14 dS m^{-1}) are very close to the TSC MAEs. The median MAE are slightly higher compared to the TSC errors in 2002 (3.36 dS m^{-1}) and notably higher in 2004 (4.49 dS m^{-1}). The 95th percentile MAE for the t-ANOCOVA estimations were 3.76 dS m^{-1} (1999), 5.48 dS m^{-1} (2002), 7.14 dS m^{-1} (2004), and 5.28 dS m^{-1} (2011). The median time-specific t-ANOCOVA intercepts were 2.01 (standard deviation, s.d., 0.08 dS m^{-1}) in 1999, 2.09 (s.d. 0.13 dS m^{-1}) in 2002, 2.05 (s.d. 0.18 dS m^{-1}) in 2004, and 2.50 (s.d. 0.11 dS m^{-1}) in 2011.

The t-ANOCOVA slope (i.e., Eq. (5)) is the exponent in the non-linear EC_e-EC_a relationship. Eq. (5) is an experimental fit of the EC_e-EC_a relationship in the range of EC_e values observed in 2012. It is likely that the slope of Eq. (5) is not representative of the EC_e-EC_a relationship over a different EC_e range. The 2012 EC_e values (min = 5.7 dS m^{-1}, mean = 20.9 dS m^{-1}, max = 38.6 dS m^{-1}, and s.d. = 7.0 dS m^{-1}) were similar to those of 1999 (min = 12.8 dS m^{-1}, mean = 20.3 dS m^{-1}, max = 36.6 dS m^{-1}, and s.d. = 5.1 dS m^{-1}), slightly smaller than those of 2011 (min = 6.3 dS m^{-1}, mean = 22.5 dS m^{-1}, max = 41.3 dS m^{-1}, and s.d. = 7.7 dS m^{-1}), and higher than those of

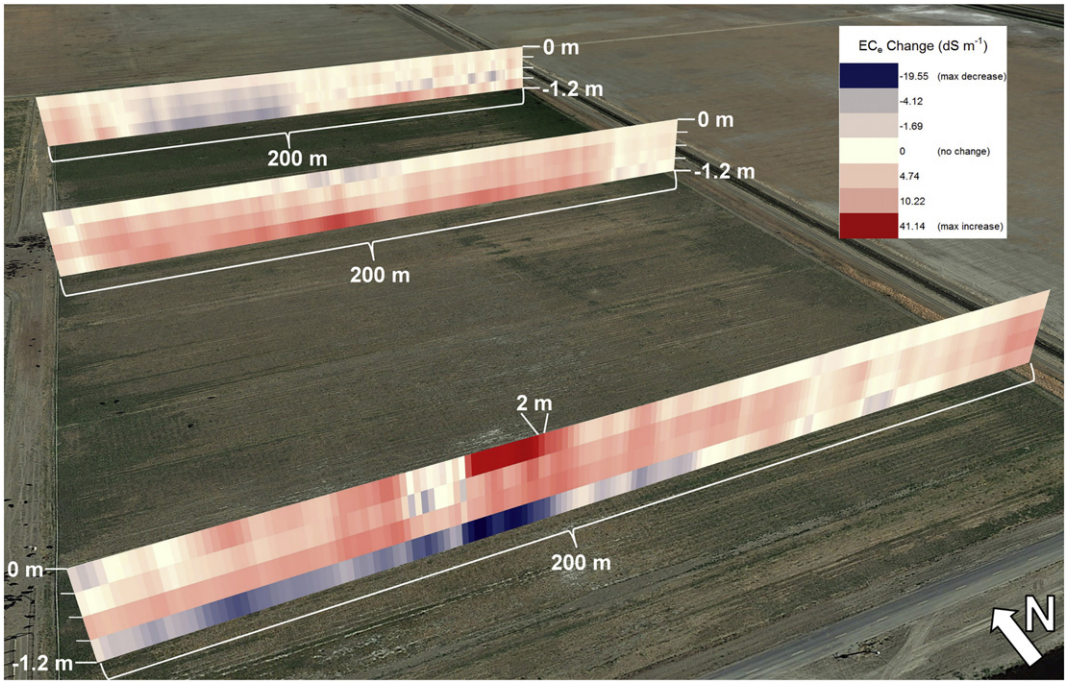

Fig. 3. 2002–2011 soil salinity (EC_e) changes at three selected parallel 1.2-m deep profiles. The cross-sections have horizontal resolution of 2 m and vertical resolution of 0.3 m. Google Earth™ imagery captured on 5/2/2015. Eye altitude is 239 m.

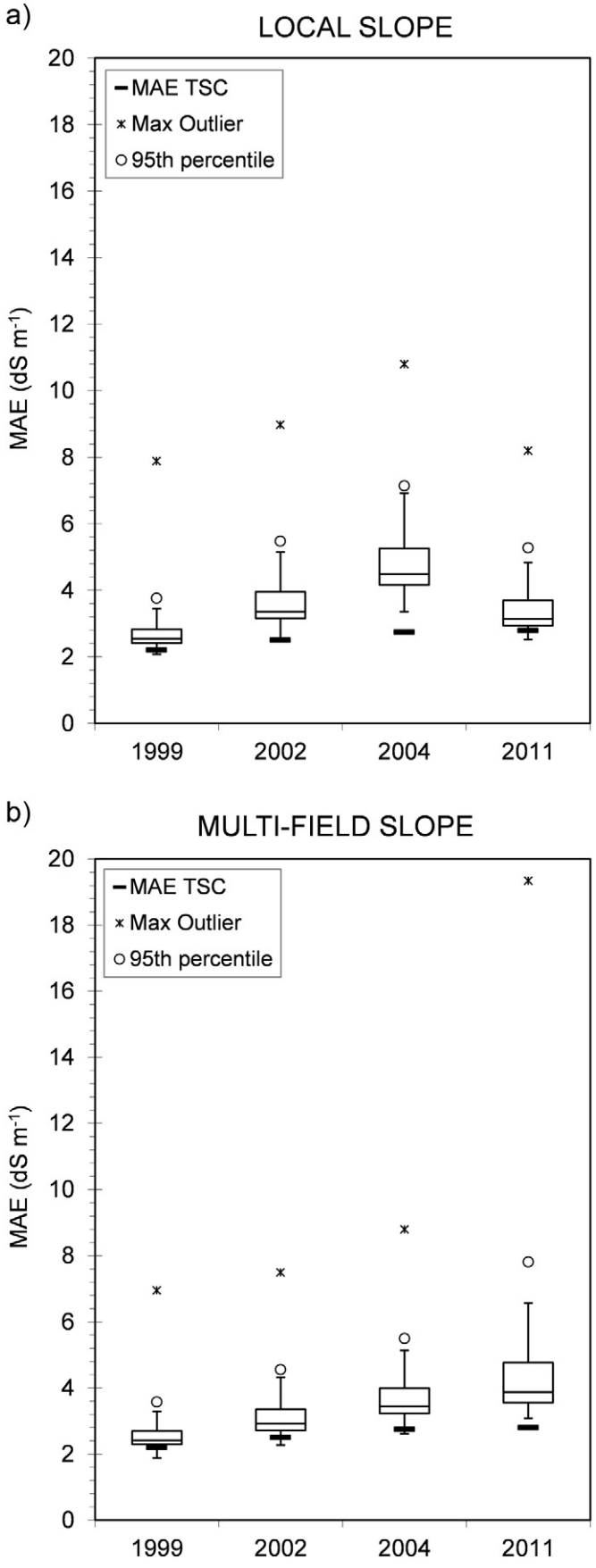

2002 (min = 7 dS m^{-1}, mean = 19.0 dS m^{-1}, max = 34.6 dS m^{-1}, and s.d. = 5.9 dS m^{-1}) and 2004 (min = 4.6 dS m^{-1}, mean = 18.1 dS m^{-1}, max = 38.6 dS m^{-1}, and s.d. = 7.8 dS m^{-1}). Thus, the greater the differences in the salinity dataset from that of 2012, the higher the t-ANOCOVA validation errors in Fig. 4a. We conclude that if a local slope is used, then it is valid only to describe the EC_e-EC_a relationship over the observed EC_e range associated with the local slope.

When a multi-field slope was used, the overall performances of the t-ANOCOVA approach improved for all years but 2011. The median MAE values were 2.42 dS m^{-1} (1999), 2.92 dS m^{-1} (2002), 3.44 dS m^{-1} (2004), and 3.88 dS m^{-1} (2011). The 95th percentile MAE for the t-ANOCOVA estimations were 3.58 dS m^{-1} (1999), 4.56 dS m^{-1} (2002), 5.50 dS m^{-1} (2004), and 7.82 dS m^{-1} (2011). The median time-specific t-ANOCOVA intercepts were 1.44 (s.d. 0.07 dS m^{-1}) in 1999, 1.61 (s.d. 0.11 dS m^{-1}) in 2002, 1.59 (s.d. 0.14 dS m^{-1}) in 2004, and 2.16 (s.d. 0.12 dS m^{-1}) in 2011. The multi-field ANOCOVA slope was calculated using the 2012 survey at the target field and EC_e-EC_a data from the twenty-one fields across the WSJV. The range of EC_e in the multi-field dataset was much wider (minimum = 0.4 dS m^{-1}; average = 11.2 dS m^{-1}; maximum = 38.6 dS m^{-1}; s.d. = 7.9 dS m^{-1}) than that of the 2012 survey for the study site. This is probably why the t-ANOCOVA validation errors are lower in Fig. 4b than in 4a. Most data points with $EC_e > 25$ dS m^{-1} in the Scudiero et al. (2016) dataset were from the field discussed in this manuscript. The 2011 survey had slightly higher salinity values than that dataset, probably causing the increase of errors of the t-ANOCOVA predictions for that year using the multi-field slope rather than the local. In this paper, the multi-field slope was obtained from a regional scale salinity assessment study (Scudiero et al., 2016). However, in practical applications, it could be obtained from a group of contiguous fields (e.g., an entire farm), as done for the Broadview Water District by Corwin and Lesch (2014).

To properly compare the performance of TSC and (multi-field slope) t-ANOCOVA EC_e estimations, Fig. 5 reports the MAEs at the 60 locations sampled in 2002 (minimum = 8.4 dS m^{-1}; average = 19.7 dS m^{-1}; maximum = 32.5 dS m^{-1}; s.d. = 6.3 dS m^{-1}) and used here as independent validation. The MAE obtained with the TSC calibration was 2.26 dS m^{-1}. For this independent validation set, the t-ANOCOVA estimations were calculated using the 9880 time-specific intercepts (for year 2002) calculated from the 40 soil samples. The median MAE for the t-ANOCOVA was 2.68 dS m^{-1}. The slight difference between the two values supports the use of the t-ANOCOVA approach, as very similar levels of EC_e prediction accuracy were obtained, but the t-ANOCOVA used substantially fewer soil samples.

When modeling log-transformed data, the error component, when back-transformed, is a function of the ratio between EC_e and the explanatory term of the equation (Baskerville, 1972; Tian et al., 2013). Large errors at high salinity values should be expected. For a close look at the t-ANOCOVA performances, let us consider the 2011 survey, when the multi-field slope provided the highest t-ANOCOVA validation errors. Fig. 6 shows the back-transformed observed-predicted EC_e relationships for the 37 validation points. In particular, re-sampling iterations yielding the 50th (Fig. 6a), 75th (Fig. 6b), and 95th (Fig. 6c) percentile of the MAE distribution are shown. The t-ANOCOVA MAEs were 3.89 dS m^{-1} (50th percentile), 4.77 dS m^{-1} (75th percentile), and 7.79 dS m^{-1} (95th percentile). The high MAE values are mainly due to larger errors for predictions of EC_e at >20–25 dS m^{-1}. It is important

Fig. 4. The t-ANOCOVA performance when using a) local (i.e., field specific) and b) multi-field slope parameter values. The boxplots represent the distribution of the mean absolute error (MAE) values of the back-transformed observed-predicted soil salinity at thirty-seven independent validation locations, obtained from the 9880 t-ANOCOVA iterations, for each year. The bottom of the rectangles corresponds to the 25th percentile, the top to the 75th. The line crossing the rectangles represents the median value. The whiskers endpoints correspond to 1.5 times the interquartile range. Circles represent the 95th percentile values. Asterisks represent maximum outliers. For comparison, the time-specific calibration (TSC) MAE values are depicted.

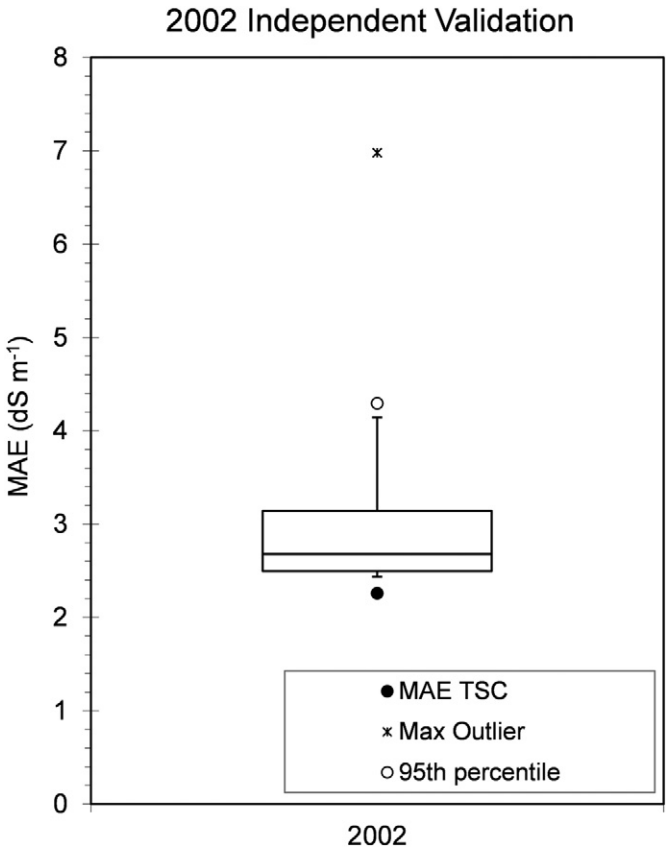

Fig. 5. Mean absolute errors (MAEs) for the 2002 t-ANOCOVA (with multiple-field slopes) salinity predictions at the 60 independent soil sampling locations. The independent MAE obtained when estimating salinity using a time-specific calibration (TSC) is reported with the black dot.

to note, that low errors are always associated with low salinity values, which is very relevant when dealing with agronomically important ranges of soil salinity. The results suggest that the t-ANOCOVA approach can be very reliable, but only at low salinity values. For 2011, when the observed data points with $EC_e > 20$ dS m^{-1} (i.e., 22 sampling locations) were excluded from the t-ANOCOVA estimations, then the validation MAEs decreased to 2.30 dS m^{-1} (5th percentile), 2.47 dS m^{-1} (25th percentile), 2.70 dS m^{-1} (50th percentile), 3.14 dS m^{-1} (75th percentile), and 4.58 dS m^{-1} (95th percentile).

4.4. Conclusions

In this paper, we reviewed how to use geospatial measurements of EC_a to *i*) infer the frequency distribution of EC_e at a target site and *ii*) to map salinity and its changes over time, providing spatiotemporal information. The first approach can be used when monitoring salinity changes over homogeneously-managed farmland, such as an entire field or a portion of it. Site-specific irrigation (e.g., Liang et al. [2016]) can be used to manage salinity, by applying different amounts and rates of water over fairly homogeneous sections of a field, also known as site-specific management units (SSMUs). The salinity changes at each SSMU can be monitored using EC_a-directed soil sampling. The second approach is useful when spatially continuous information is needed over an entire field: for example, when the response of crop health (e.g., measured with remote sensing) to spatial changes of salinity is investigated. Both methodologies rely on the use of several (e.g., dozens) soil samples to infer salinity and/or to calibrate EC_a measurements.

Due to the reduced labor costs, the t-ANOCOVA approach can be used to monitor spatiotemporal salinity changes in the root-zone (e.g. 0–1.2 m) at reasonably high temporal resolution. This approach is based on the notion that the EC_e-EC_a relationship can be described with a power (nonlinear) model. When this relationship is log transformed, a general slope coefficient can be used to estimate EC_e from EC_a measurements for an entire farmland (or region). At each monitoring date, a field-specific intercept is calculated from as few as three sampling locations. When the t-ANOCOVA slope is properly calibrated, the salinity estimations in the ranges of interest for agronomical production ($EC_e < 20$ dS m^{-1}) are reasonably accurate. However, as shown in Fig. 4, estimates having large errors may be generated using this approach.

A future experiment to validate the t-ANOCOVA methodology could be done by monitoring salinity changes over multiple irrigated fields with salinity ranging from 0 to 20–30 dS m^{-1}. Initially, a farm-wide t-ANOCOVA slope should be calculated. Then, at subsequent EC_a surveys, three random soil sampling locations should be used for the calibration of the field-specific t-ANOCOVA intercept. A few (e.g., 10) validation points per field should be selected, to assess the quality of the t-ANOCOVA predictions. To understand the t-ANOCOVA strengths and limitations, the study should compare the t-ANOCOVA independent validation errors with TSC independent validations over the same locations. The EC_a surveys should follow consistent protocols discussed by Corwin and Scudiero (2016), with particular attention to soil temperature and carrying out the surveys at comparable soil water contents. In fields characterized by high spatial variability of soil texture, bulk density, and other soil properties that influence the EC_a measurements, ancillary information from other soil sensors, such as gamma-ray and visible/near-infrared spectroscopy, could be integrated in Eq. (2) to

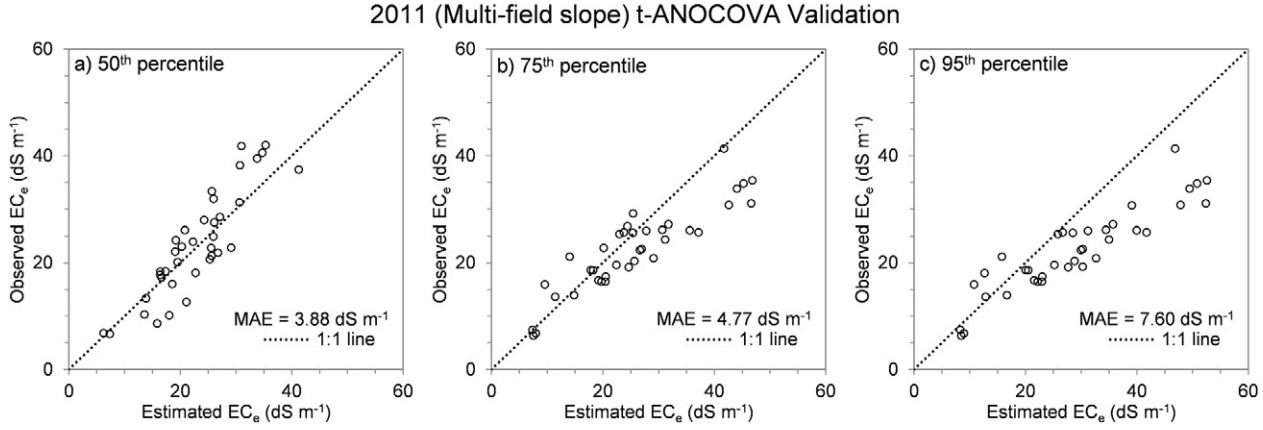

Fig. 6. Observed-predicted salinity (EC_e) relationships for the t-ANOCOVA validation iterations providing the a) 50th, b) 75th, and c) 95th percentiles of the mean absolute error (MAE).

increase the accuracy of EC_e predictions:

$$EC_e = \delta \times EC_a^{\alpha} \times \Omega^{\zeta} \times \varepsilon^{*} \quad (6)$$

where Ω is soil sensor data used as a proxy for texture, or any other quantitative indicator of soil type found to influence EC_a in the area of interest, and α, ζ, and δ are the model coefficients. The α and ζ coefficients should be estimated during the initial multi-field calibration, whereas δ should be estimated, at each field, every time salinity is measured.

If validated, the t-ANOCOVA approach would be beneficial to farmers, agricultural consultants, and other stakeholders. In arid and semi-arid agricultural areas where water resources for irrigation are increasingly limited and of lower quality (i.e., of higher salinity), monitoring spatiotemporal variations of soil salinity in a timely and inexpensive fashion will be essential to preserving the long-term sustainability of agricultural production.

Acknowledgements

The authors wish to acknowledge the numerous hours of diligent technical work that was performed in the field and in the laboratory by Michael Bagtang, Harry Forster, Jack Jobes, Clay Wilkinson, and Kevin Yemoto, whose efforts and conscientiousness were crucial to the success of the project.

References

Achen, C.H., 1982. Interpreting and using regression. Sage, Beverly Hills, CA, USA.
Allred, B.J., Groom, D., Reza Eshani, M., Daniels, J.J., 2008. Resistivity methods. In: Allred, B.J., Daniels, J.J., Reza Ehsani, M. (Eds.), Handbook of agricultural geophysics. CRC Press, Taylor & Francis Group, New York, NY, USA.
Archie, G.E., 1942. The electrical resistivity log as an aid in determining some reservoir characteristics. Trans. AIME 5, 54–62.
Arroues, K.D., Anderson, J.C.H., 1986. Soil survey of Kings County California. USDA. Soil Conservation Service, Washington, DC 212 pp.
Baskerville, G., 1972. Use of logarithmic regression in the estimation of plant biomass. Can. J. For. Res. 2, 49–53.
Cliff, A.D., Ord, J.K., 1981. Spatial processes: models & applications. Pion, London, UK.
Cordioli, M., Pironi, C., De Munari, E., Marmiroli, N., Lauriola, P., Ranzi, A., 2017. Combining land use regression models and fixed site monitoring to reconstruct spatiotemporal variability of NO_2 concentrations over a wide geographical area. Sci. Total Environ. 574, 1075–1084.
Corwin, D.L., 2012. Field-scale monitoring of the long-term impact and sustainability of drainage water reuse on the west side of California's San Joaquin Valley. J. Environ. Monit. 14, 1576–1596.
Corwin, D.L., Lesch, S.M., 2003. Application of soil electrical conductivity to precision agriculture. Agron. J. 95, 455–471.
Corwin, D.L., Lesch, S.M., 2005. Apparent soil electrical conductivity measurements in agriculture. Comput. Electron. Agric. 46, 11–43.
Corwin, D.L., Lesch, S.M., 2013. Protocols and guidelines for field-scale measurement of soil salinity distribution with EC_a-directed soil sampling. J. Environ. Eng. Geophys. 18, 1–25.
Corwin, D.L., Lesch, S.M., 2014. A simplified regional-scale electromagnetic induction—Salinity calibration model using ANOCOVA modeling techniques. Geoderma 230–231, 288–295.
Corwin, D.L., Lesch, S.M., 2016. Validation of the ANOCOVA model for regional-scale EC_a-EC_e calibration. Soil Use Manag. http://dx.doi.org/10.1111/sum.12262.
Corwin, D.L., Scudiero, E., 2016. Field-scale apparent soil electrical conductivity. In: Logsdon, S. (Ed.), Methods of soil analysis. vol. 1. Soil Science Society of America, Madison, WI, USA. http://dx.doi.org/10.2136/methods-soil.2015.0038.55.
Corwin, D.L., Kaffka, S.R., Hopmans, J.W., Mori, Y., Van Groenigen, J.W., Van Kessel, C., et al., 2003. Assessment and field-scale mapping of soil quality properties of a saline-sodic soil. Geoderma 114, 231–259.
Corwin, D.L., Lesch, S.M., Oster, J.D., Kaffka, S.R., 2008. Short-term sustainability of drainage water reuse: Spatio-temporal impacts on soil chemical properties. J. Environ. Qual. 37, S-8–S-24.
Doolittle, J.A., Brevik, E.C., 2014. The use of electromagnetic induction techniques in soils studies. Geoderma 223, 33–45.
FAO, ITPS, 2015. State of the world's soil resources. Main report. Food and Agriculture Organization of the United Nations and Intergovernmental Technical Panel on Soils, Rome, Italy.
Farahani, H., Buchleiter, G., 2004. Temporal stability of soil electrical conductivity in irrigated sandy fields in Colorado. Trans. ASAE 47, 79–90.
Fitzgerald, G.J., Lesch, S.M., Barnes, E.M., Luckett, W.E., 2006. Directed sampling using remote sensing with a response surface sampling design for site-specific agriculture. Comput. Electron. Agric. 53, 98–112.
Guo, Y., Shi, Z., Huang, J., Zhou, L., Zhou, Y., Wang, L., 2015. Characterization of field scale soil variability using remotely and proximally sensed data and response surface method. Stoch. Env. Res. Risk A. 30, 859–869.
Hengl, T., Rossiter, D.G., Stein, A., 2003. Soil sampling strategies for spatial prediction by correlation with auxiliary maps. Aust. J. Soil Res. 41, 1403–1422.
Hengl, T., Heuvelink, G.B., Stein, A., 2004. A generic framework for spatial prediction of soil variables based on regression-kriging. Geoderma 120, 75–93.
Huang, J., Prochazka, M.J., Triantafilis, J., 2016. Irrigation salinity hazard assessment and risk mapping in the lower Macintyre Valley, Australia. Sci. Total Environ. 551, 460–473.
Lesch, S.M., 2005. Sensor-directed response surface sampling designs for characterizing spatial variation in soil properties. Comput. Electron. Agric. 46, 153–179.
Lesch, S.M., 2012. Statistical models for the prediction of field-scale and spatial salinity patterns from soil conductivity survey data. In: Wallender, W.W., Tanji, K.K. (Eds.), Agricultural salinity assessment and management. ASCE, Reston, VA, USA.
Lesch, S.M., Corwin, D.L., 2008. Prediction of spatial soil property information from ancillary sensor data using ordinary linear regression: model derivations, residual assumptions and model validation tests. Geoderma 148, 130–140.
Lesch, S.M., Rhoades, J.D., Lund, L.J., Corwin, D.L., 1992. Mapping soil salinity using calibrated electromagnetic measurements. Soil Sci. Soc. Am. J. 56, 540–548.
Lesch, S.M., Rhoades, J.D., Corwin, D.L., 2000. ESAP-95 version 2.01 R. User manual and tutorial guide. US Salinity Laboratory, Riverside, CA, USA.
Liang, X., Liakos, V., Wendroth, O., Vellidis, G., 2016. Scheduling irrigation using an approach based on the van Genuchten model. Agric. Water Manag. 176, 170–179.
Nelson, M., Bishop, T., Triantafilis, J., Odeh, I., 2011. An error budget for different sources of error in digital soil mapping. Eur. J. Soil Sci. 62, 417–430.
Odeh, I.O., McBratney, A., Chittleborough, D., 1995. Further results on prediction of soil properties from terrain attributes: heterotopic cokriging and regression-kriging. Geoderma 67, 215–226.
Pedrera-Parrilla, A., Brevik, E.C., Giráldez, J.V., Vanderlinden, K., 2016. Temporal stability of electrical conductivity in a sandy soil. Int. Agrophys. 30, 349–357.
Rhoades, J.D., Raats, P.A.C., Prather, R.J., 1976. Effects of liquid-phase electrical conductivity, water content, and surface conductivity on bulk soil electrical conductivity. Soil Sci. Soc. Am. J. 40, 651–655.
Rhoades, J., Manteghi, N., Shouse, P., Alves, W., 1989. Soil electrical conductivity and soil salinity: new formulations and calibrations. Soil Sci. Soc. Am. J. 53, 433–439.
Scudiero, E., Skaggs, T.H., Corwin, D.L., 2016. Comparative regional-scale soil salinity assessment with near-ground apparent electrical conductivity and remote sensing canopy reflectance. Ecol. Indic. 70, 276–284.
Tanji, K.K., Wallender, W.W., 2012. Nature and extent of agricultural salinity and sodicity. In: Wallender, W.W., Tanji, K.K. (Eds.), Agricultural Salinity Assessment and Management. ASCE Manuals and Reports on Engineerring Practices No. 71. ASCE, Reston, VA, USA.
Tian, Y., Huffman, G.J., Adler, R.F., Tang, L., Sapiano, M., Maggioni, V., et al., 2013. Modeling errors in daily precipitation measurements: additive or multiplicative? Geophys. Res. Lett. 40, 2060–2065.
Van Noten, K., 2016. Visualizing cross-sectional data in a real-world context. Eos 97, 16–19.
Wicke, B., Smeets, E., Dornburg, V., Vashev, B., Gaiser, T., Turkenburg, W., et al., 2011. The global technical and economic potential of bioenergy from salt-affected soils. Energy Environ. Sci. 4, 2669–2681.
Williams, A.P., Seager, R., Abatzoglou, J.T., Cook, B.I., Smerdon, J.E., Cook, E.R., 2015. Contribution of anthropogenic warming to California drought during 2012–2014. Geophys. Res. Lett. 42, 6819–6828.